Low-mass doubly charged Higgs bosons at the LHC

Saiyad Ashanujjaman,[1,2,3,*] Kirtiman Ghosh,[1,4,†] and Rameswar Sahu[1,4,‡]

[1]*Institute of Physics, Bhubaneswar, Sachivalaya Marg, Sainik School, Bhubaneswar 751005, India*
[2]*Department of Physics, SGTB Khalsa College, Delhi 110007, India*
[3]*Department of Physics and Astrophysics, University of Delhi, Delhi 110007, India*
[4]*Homi Bhabha National Institute, Training School Complex, Anushakti Nagar, Mumbai 400094, India*

(Received 3 November 2022; accepted 3 January 2023; published 23 January 2023)

Search for light (within the mass range 84–200 GeV) doubly charged Higgs bosons decaying into a pair of W bosons has been deemed challenging using the conventional LHC searches with leptons, jets, and missing transverse momentum in the final state. Such Higgses, together with slightly heavier singly-charged and neutral Higgses, when arranged in an $SU(2)_L$ triplet as in the type-II seesaw model, have been recently shown to accommodate the recent measurement of the W-boson mass by the CDF Collaboration. When produced in a highly Lorentz-boosted regime, these tend to manifest as a single fat jet or a pair of adjacent same-sign leptons plus missing transverse momentum. First, we perform a multivariate analysis to discern such exotic jets from the standard model jets. Then, we present a novel search in the final state with an exotic jet and two same-sign leptons plus missing transverse momentum. We find that such low-mass doubly charged Higgses could be directly probed with the already collected Run 2 LHC data.

DOI: 10.1103/PhysRevD.107.015018

I. INTRODUCTION

Despite being remarkably successful in understanding particle physics phenomenology, the Standard Model (SM) in its present form lacks a mass term for neutrinos. However, a trivial Dirac mass term for the neutrinos can be effectuated by dint of the usual Higgs mechanism by introducing right-handed neutrinos to the SM. Although plausible, this warrants philosophical displeasure as it calls for diminutive Yukawa couplings. Conversely, a well-founded remedy to this menace is offered by the so-called *seesaw mechanism*, wherein a lepton number violating new physics beyond the SM is invoked at an *a priori* unknown scale—presumably away from both the electroweak (EW) scale and the Planck scale, so that on integrating out the heavy fields the SM neutrinos are left with the observed sub-eV masses after the EW symmetry breaking. Pointedly, numerous models of varying complexity and collider testability have been proposed over the last few decades. The type-II seesaw model [1–6], a UV completion of the Weinberg operator at the tree level [7,8], extending the SM with an $SU(2)_L$ triplet scalar field with hypercharge $Y = 1$, is arguably the most widely studied variant [9–62]. For one, the flavor structure of the Yukawa coupling driving the leptonic decays of the tripletlike scalars ensues being governed by the neutrino oscillation data up to the scalar triplet vacuum expectation value (VEV). Moreover, the presence of the doubly charged scalars ($H^{\pm\pm}$) and their characteristic decays to a pair of same-sign leptons ($\ell^\pm\ell^\pm$) or W bosons offer interesting ways to probe them directly at the current and near-future experiments.

The experimental collaborations have carried out several searches for $H^{\pm\pm}$ [63–73], and nonobservations of any significant excess over the SM expectations have led to stringent limits on them. For $H^{\pm\pm}$ decaying into $\ell^\pm\ell^\pm$, the ATLAS Collaboration has set a lower limit of 1020 GeV, assuming equal branching fractions across modes [73]. This search considers only light leptons in the final states and thus is not sensitive for $H^{\pm\pm}$ decaying into $\tau^\pm\tau^\pm$. The CMS Collaboration has set a lower limit of 535 GeV on such scalars [68]. For $H^{\pm\pm}$ decaying into $W^\pm W^\pm$, the ATLAS Collaboration has excluded them within the mass range 200–350 GeV [72]. An orderly reinterpretation of this search considering all possible Drell-Yan production modes for the tripletlike scalars results in an improved exclusion range of 200–400 GeV [60]. Moreover, a reinterpretation of the ATLAS same-sign dilepton search in Ref. [65] has derived an exclusion limit of 84 GeV [37].

In a nutshell, $H^{\pm\pm}$ decaying into $WW^{(*)}$ are still allowed in the 84–200 GeV mass window. In this mass window, the

*saiyad.a@iopb.res.in
†kirti.gh@gmail.com
‡rameswar.s@iopb.res.in

type-II seesaw model predicts a cross section between 1.5 pb and 65 fb for $pp \to H^{++}H^{--}$ at the 13 TeV LHC. Despite a sizeable cross section, searching such an $H^{\pm\pm}$ using the conventional LHC searches with leptons, jets, and missing transverse momentum in the final state has been deemed challenging. Presumably, for one, their eventual decay products tend to be not so hard and are likely to be drowned in the LHC environment, owing to the inherent towering EW and QCD backgrounds. Moreover, ineludible contamination from the SM resonances makes the state of affairs worse. To the extent of our knowledge, the only notable effort in probing this mass window was made in Ref. [74]. Lately, Refs. [75–78] have demonstrated that the recently reported measurement of the W-boson mass by the CDF experiment [79] which substantially differs from the global EW fit [80] can be explained within the type-II seesaw model predicting such low-mass $H^{\pm\pm}$ and slightly heavier singly-charged and neutral scalars. This anomaly can also be accommodated within the Georgi-Machacek model (including two isospin triplet Higgs fields) extended with custodial symmetry-breaking terms in the potential; see Refs. [81,82]. Therefore, it is paramount to look for such $H^{\pm\pm}$ at the LHC.

In this work, we present a novel search strategy for such $H^{\pm\pm}$. We consider their pair production in a highly Lorentz-boosted regime such that they are produced back to back with large transverse momenta, manifesting themselves as a single fat jet or a pair of adjacent same-sign leptons plus missing transverse momentum. Obviously, this would reduce the signal cross section significantly. However, should we be able to discern such exotic jets from the SM jets, a final state with such a jet and two same-sign leptons plus missing transverse momentum would have a compensating advantage of reducing the SM background more aggressively, thereby ameliorating the signal-to-background ratio. Keeping that in mind, first, we perform a multivariate analysis incorporating the jet mass, jet charge, N-subjettiness, etc., variables as inputs to the boosted decision tree (BDT) classifier to discern such exotic jets (dubbed $H^{\pm\pm}$ jets hereafter) from the SM jets. Then, we perform a search in the final state with an $H^{\pm\pm}$ jet and two same-sign leptons plus missing transverse momentum.

The rest of this work is structured as follows. In Sec. II, we briefly discuss the doubly charged Higgses in the type-II seesaw model. We perform a detailed collider analysis in Sec. III. Finally, we summarize in Sec. IV.

II. DOUBLY CHARGED HIGGSES

In the type-II seesaw model, the SM is augmented with an $SU(2)_L$ triplet scalar field with hypercharge $Y = 1$,

$$\Delta = \begin{pmatrix} \Delta^+/\sqrt{2} & \Delta^{++} \\ \Delta^0 & -\Delta^+/\sqrt{2} \end{pmatrix}. \tag{1}$$

The scalar potential involving Δ and the SM Higgs doublet $\Phi = (\Phi^+ \Phi^0)^T$ is given by

$$\begin{aligned} V(\Phi,\Delta) = &-m_\Phi^2 \Phi^\dagger\Phi + \frac{\lambda}{4}(\Phi^\dagger\Phi)^2 + m_\Delta^2 \mathrm{Tr}(\Delta^\dagger\Delta) \\ &+ [\mu(\Phi^T i\sigma^2 \Delta^\dagger \Phi) + \mathrm{H.c.}] + \lambda_1 (\Phi^\dagger\Phi)\mathrm{Tr}(\Delta^\dagger\Delta) \\ &+ \lambda_2 [\mathrm{Tr}(\Delta^\dagger\Delta)]^2 + \lambda_3 \mathrm{Tr}[(\Delta^\dagger\Delta)^2] + \lambda_4 \Phi^\dagger \Delta\Delta^\dagger \Phi, \end{aligned} \tag{2}$$

where m_Φ^2, m_Δ^2, and μ are the mass parameters; λ and λ_i $(i = 1, \ldots, 4)$ are the dimensionless quartic couplings; and σ^2 is one of the Pauli matrices. The neutral components Φ^0 and Δ^0 procure respective VEVs v_d and v_t such that $\sqrt{v_d^2 + 2v_t^2} = 246$ GeV. After the EW symmetry is broken, the degrees of freedom carrying identical electric charges mix, thereby resulting in several physical Higgs states:

(1) The neutral states Φ^0 and Δ^0 mix into two CP-even and two CP-odd states (h and H^0 and G^0 and A^0).
(2) The singly-charged states $\Phi^\pm$ and $\Delta^\pm$ mix into two mass states $G^\pm$ and $H^\pm$.
(3) The doubly charged state $\Delta^{\pm\pm}$ is aligned with its mass state $H^{\pm\pm}$.

The mass states G^0 and $G^\pm$ are the *would-be* Nambu-Goldstone bosons, h is identified as the 125 GeV Higgs observed at the LHC, and the rest follows the sum rule

$$m_{H^{\pm\pm}}^2 - m_{H^\pm}^2 \approx m_{H^\pm}^2 - m_{H^0/A^0}^2 \approx -\frac{\lambda_4}{4} v_d^2. \tag{3}$$

The main dynamical features of the scalar potential—in particular, the tree-level unitarity constraints as well as the boundedness from below constraints on the scalar couplings—have been studied in detail in Refs. [23,27,30,43,46]. When combined, these constraints delineate the theoretically allowed parameter space within the perturbative approximation regime. Reference [23] shows that the mass of the lighter CP-even state must satisfy a theoretical upper bound of ∼1 TeV (which is trivially satisfied when the lighter CP-even state is identified as the 125 GeV Higgs observed at the LHC), while the upper bound for the remaining Higgses extends up to several tens of TeV. In Fig. 1, we show the theoretically allowed parameter space in the plane of $m_{H^{\pm\pm}}$ and $\Delta m = m_{H^{\pm\pm}} - m_{H^\pm}$ for $v_t = 1$ GeV. This work focuses on $H^{\pm\pm}$ in the 84–200 GeV mass range, which is theoretically allowed as long as Δm is less than few tens of GeV. However, note that the present work is largely insensitive to Δm and v_t, and thus do not commit to any fixed value for them.

The Yukawa interaction $Y_{ij}^\nu L_i^T C i\sigma^2 \Delta L_j$ (L_i stands for the SM lepton doublet with $i \in e, \mu, \tau$, and C stands for

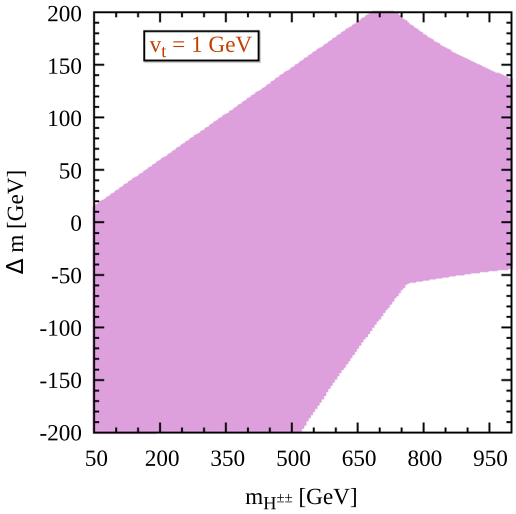

FIG. 1. Theoretically allowed $m_{H^{\pm\pm}}$-Δm parameter space for $v_t = 1$ GeV.

the charge-conjugation operator) induces masses for the neutrinos:

$$m_\nu = \sqrt{2} Y^\nu v_t. \tag{4}$$

The doubly charged Higgses are pair produced aplenty at the LHC by quark-antiquark annihilation via the neutral current Drell-Yan mechanism[1]:

$$q\bar{q} \to \gamma^*/Z^* \to H^{++}H^{--}.$$

We evaluate the leading order (LO) cross sections using the SARAH 4.14.4 [83,84] generated UFO [85] modules in MadGraph5_aMC_v2.7.3 [86,87] with the NNPDF23_lo_as_0130_qed parton distribution function [88,89]. Figure 2 shows the LO doubly charged Higgs pair production cross section at the 13 TeV LHC as a function of their mass. Following the relevant QCD corrections estimated in Refs. [13,90], we naively scale the LO cross section by an overall next-to-leading (NLO) K factor of 1.15. Therefore, the resulting $pp \to H^{++}H^{--}$ cross section varies from 1.72 pb to 74.5 fb for 84 to 200 GeV mass.

After being produced, $H^{\pm\pm}$ decays into $\ell^\pm\ell^\pm$, $W^\pm W^{\pm(*)}$, and $H^\pm W^{\pm *}$, if kinematically allowed. In broad terms, the dominance of one decay mode over the others depends on three parameters, namely, $m_{H^{\pm\pm}}$, v_t, and $\Delta m = m_{H^{\pm\pm}} - m_{H^\pm}$; see Refs. [20,25,60] for detailed discussions. For the present work, without committing to a fixed value for v_t and Δm, we assume exclusive prompt decays of $H^{\pm\pm}$ to $W^\pm W^{\pm(*)}$.

[1]They are also produced via t/u-channel photon fusion as well as vector-boson fusion processes. However, such processes are rather subdominant.

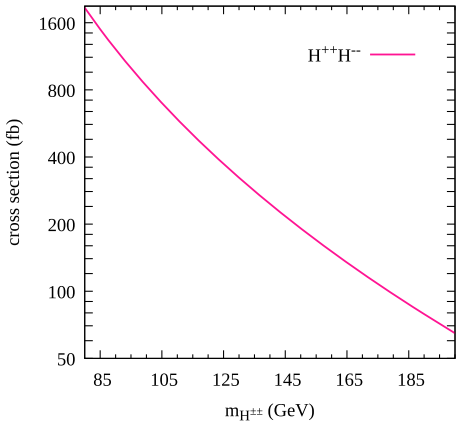

FIG. 2. LO $pp \to H^{++}H^{--}$ cross section at the 13 TeV LHC.

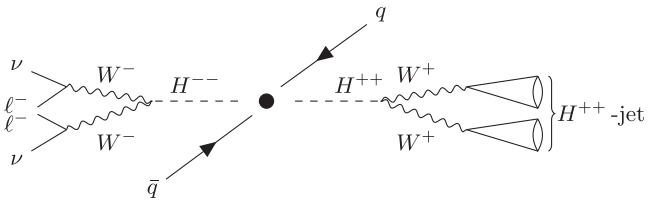

FIG. 3. Schematic Feynman diagram for $q\bar{q} \to H^{++}H^{--}$ and its subsequent decays to one $H^{\pm\pm}$ jet, two same-sign leptons, and neutrinos.

III. COLLIDER ANALYSIS

In this section, we present a novel search strategy for $H^{\pm\pm}$ with $m_{H^{\pm\pm}} \in [84\text{–}200]$ GeV. We only consider $H^{\pm\pm}$ which are produced in a highly Lorentz-boosted regime, manifesting themselves as a single fat jet or a pair of adjacent same-sign leptons plus missing transverse momentum. Such a requirement significantly reduces the signal cross section.[2] As argued earlier, despite such a notable reduction in the signal cross section, the final state with an $H^{\pm\pm}$ jet and two same-sign leptons plus missing transverse momentum (see Fig. 3) is expected to have a compensating advantage of reducing the SM background more aggressively with the proviso that we discern the $H^{\pm\pm}$ jets from the SM jets.

In the following, we briefly describe the reconstruction and selection of various physics objects, then perform a multivariate analysis to discern the $H^{\pm\pm}$ jets from the SM jets, viz., QCD jets, W/Z jets, h jets, and t jets, and finally delineate a search in the final state with an $H^{\pm\pm}$ jet and two same-sign leptons plus missing transverse momentum.

A. Object reconstruction and selection

We pass the parton-level events into PYTHIA 8.2 [91] to simulate subsequent decays for the unstable particles,

[2]For example, a parton-level cut of $p_T(H^{\pm\pm}) > 300$ GeV reduces the $pp \to H^{++}H^{--}$ cross section by a factor of 48 (4.4) to 37.4 (17.0) fb for $m_{H^{\pm\pm}} = 84(200)$ GeV.

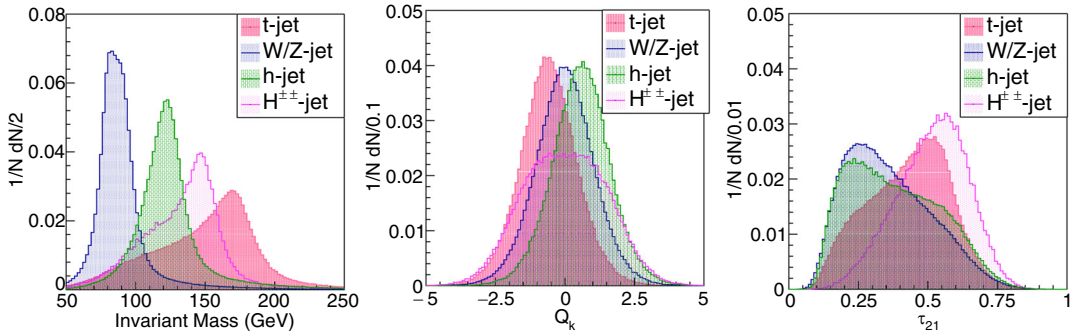

FIG. 4. Normalized distributions for some of the input features. The signal distributions are for $m_{H^{\pm\pm}} = 150$ GeV.

initial- and final-state radiation (ISR and FSR), showering, fragmentation, and hadronization and then into DELPHES 3.4.2 with the default CMS card [92] for simulating detector effects as well as reconstructing various physics objects, viz., photons, electrons, muons, and jets.

Constituents of the would-be fat jets are clustered using the *anti-k_T algorithm* [93] with a characteristic jet radius $R = 1.0$ as implemented in FastJet 3.3.2 [94]. To remove the soft yet wide-angle QCD emissions from the fat jets, we use the *jet pruning* algorithm [95,96] with the default values for the pruning parameters: $z_{\rm cut} = 0.1$ and $R_{\rm cut} = 0.5$ [95]. Further, to unfold the multiprong nature of the fat jets, we use an inclusive jet shape termed as *N-subjettiness* τ_N [97,98][3] choosing *one-pass k_T axes* for the minimisation procedure and $\beta = 1$. Reconstructed jets are required to be within the pseudorapidity range $|\eta| < 2.5$ and have a transverse momentum $p_T > 30$ GeV, whereas the leptons (electrons and muons) are required to have $|\eta| < 2.5$ and $p_T > 10$ GeV. Moreover, we demand the scalar sum of the p_Ts of all other objects lying within a cone of radius 0.3 (0.4) around an electron (a muon) to be smaller than 10% (15%) of its p_T. This ensures that the leptons are isolated. Finally, the missing transverse momentum $\vec{p}_T^{\rm miss}$ (with magnitude $p_T^{\rm miss}$) is estimated from the momentum imbalance in the transverse direction associated to all reconstructed objects in an event.

B. Multivariate analysis: Discerning the $H^{\pm\pm}$ jets from the SM jets

Here, we perform a multivariate analysis with the BDT classifier implemented in the TMVA 4.3 toolkit [99] integrated into the analysis framework ROOT 6.24 [100]. For training and testing the classifier, we use 600,000 events for each category of the SM jets and 300,000 for each $m_{H^{\pm\pm}}$ within the [85,195] GeV range in steps of 10 GeV. Of these, 80% are picked randomly for training, and the rest are used for testing.

We use the following kinematic features of the jets as inputs to the BDT classifier:

(1) invariant mass m,
(2) b tag[4]
(3) jet charge Q_k [101][5]
(4) N-subjettiness variables τ_1, τ_{21}, τ_{32}, and τ_{43}.[6]

Normalized distributions for some of the input features are shown in Fig. 4, and the rest are not shown for brevity. These variables constitute a minimal set with (a) good discrimination power between the $H^{\pm\pm}$ jets and the SM jets and (b) low correlations among themselves. The method-unspecific separation is a good measure of the former. For a given feature x, this is defined as

$$\langle S^2 \rangle = \frac{1}{2} \int \frac{[\hat{x}_H(x) - \hat{x}_{\rm SM}(x)]^2}{\hat{x}_H(x) + \hat{x}_{\rm SM}(x)} dx, \tag{5}$$

where $\hat{x}_H(x)$ and $\hat{x}_{\rm SM}(x)$ are the probability density functions of x for the $H^{\pm\pm}$ jets and the SM jets, respectively. Table I shows method-unspecific separation for the input features, while Fig. 5 shows their Pearson's linear correlation coefficients defined as

$$\rho(x, y) = \frac{\langle xy \rangle - \langle x \rangle \langle y \rangle}{\sigma_x \sigma_y}, \tag{6}$$

where $\langle x \rangle$ and σ_x, respectively, are the expectation value and standard deviation of x.

[3]It is defined as $\tau_N = \frac{1}{d_0} \sum_k p_{T,k} \min(\Delta R^{\beta}_{1,k}, \Delta R^{\beta}_{2,k}, \ldots, \Delta R^{\beta}_{N,k})$, where N is the number of subjets a jet is presumably composed of, k runs over the jet constituents with transverse momentum $p_{T,k}$, $\Delta R_{i,k}$ is the distance in the rapidity-azimuth plane between a candidate subjet i and a jet constituent k, $d_0 = \sum_k p_{T,k} R_0^{\beta}$ with $R_0 (= 1.0)$ being the characteristic jet radius used in the original jet clustering algorithm, and β is an angular weighting exponent dubbed *thurst parameter*.

[4]It is a *Boolean* indicating whether or not at least one of the constituent subjet is a b jet.

[5]Jet charge is defined as $Q_k = \frac{\sum_i q_i (p_{T,i})^k}{\sum_i p_{T,i}}$, where i runs over the associated tracks with transverse momentum $p_{T,i}$ and charge q_i and k is a free regularisation exponent which we take to be 0.2.

[6]$\tau_{N,N-1} = \tau_N / \tau_{N-1}$ is a useful discriminant between N- and $(N-1)$-prong jets.

TABLE I. Method-unspecific separation and method-specific ranking of the input features.

Feature	Method-unspecific separation	Method-specific ranking
m	0.064	0.152
b-tag	0.099	0.167
Q_k	0.052	0.101
τ_1	0.134	0.151
τ_{21}	0.104	0.208
τ_{32}	0.075	0.120
τ_{43}	0.066	0.102

To enhance the BDT classification, we use the *adaptive boost* algorithm with a learning rate of 0.1 and combine 1000 decision trees with 5% minimum node size and a depth of four layers per tree into a forest. As for the separation criterion for node splitting, we use the so-called *Gini index*. The relevant BDT hyperparameters are summarized in Table II. Table I also shows the method-specific ranking of the input features. In other words, this shows the relative importance of the input features in separating the $H^{\pm\pm}$-jets from the SM jets. As we see from Table I, the N-subjettiness variable τ_{21} is the best separating variable, while the jet-charge Q_k is the one with least separating power. Finally, we check the classifier for overtraining by performing the Kolmogorov-Smirnov test which compares the BDT response curves for the training and testing subsamples; see Fig. 6. These response curves exhibit no considerable overtraining.

In the left panel of Fig. 7, we show the receiver-operator-characteristic (ROC) curve, which quantifies the BDT performance, for $m_{H^{\pm\pm}} = 150$ GeV. The right panel of Fig. 7 shows the signal (with $m_{H^{\pm\pm}} = 150$ GeV) and background efficiencies (ϵ_{Sig} and ϵ_{Bckg}) as a function of the BDT response.[7] The area below the ROC curve is less than 13% of the total area, indicating considerably well separation between the signal and background. For a BDT response greater than 0, not only ϵ_{Bckg} but also ϵ_{Sig} falls to lower values, whereas for a BDT response less than 0, both rises to higher values. Therefore, we choose an optimum value of 0.1 for the BDT response. For the chosen value of the BDT response, different background efficiencies are 13–20%: 17.8%, 20.4%, 13.4%, and 13.2% for t, h, W/Z, and QCD jets, respectively. In Fig. 8, we show the variation of ϵ_{Sig} with $m_{H^{\pm\pm}}$ for the same value of the BDT response. The abrupt drop in ϵ_{Sig} for $m_{H^{\pm\pm}} \lesssim 100$ GeV is ascribed to the small mass difference between $m_{H^{\pm\pm}}$ and the W mass.

[7]Note that these plots only display efficiencies due to the classifier performance and do not reflect those arising from object reconstructions and selections. For the mass range of our interest, a partonic $H^{\pm\pm}$ decaying into a pair of hadronically decaying W bosons being reconstructed and selected as a fat jet has an overall efficiency of ∼80%.

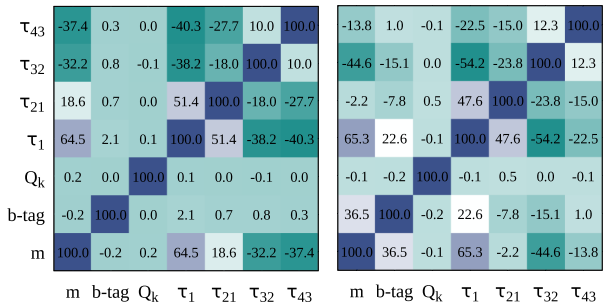

FIG. 5. Correlations in percent among the input features for the $H^{\pm\pm}$ jets (left) and the SM jets (right).

For small mass difference, the decay products of the off-shell W boson emanating from $H^{\pm\pm}$ tend to be very soft and thus are not likely to pass the object reconstruction and selection criteria discussed in Sec. III A. As a consequence of this, the features of an $H^{\pm\pm}$ jet resemble to those of an SM jet, thereby making the former indiscernible from the latter.

C. SM backgrounds

As the background for the present analysis, we consider numerous SM processes such as diboson, triboson, and tetraboson processes, Higgsstrahlung processes, single- and multitop productions in association with/without gauge bosons, and Drell-Yan processes. All these processes are generated in association with up to two jets at the LO using MadGraph5_aMC_v2.7.3 [86,87] at least of worth 3000 fb^{-1} luminosity of data at the 13 TeV LHC, followed by the so-called MLM jet matching using PYTHIA 8.2 [91], and then naively scaled by appropriate NLO (or higher, whichever is available in the literature) K factors [87,102–116].

The relevant backgrounds can be broadly classified into two classes: prompt and nonprompt. While most of these processes contribute to the former, only the processes where a jet is misidentified as a lepton or additional leptons originate from ISR/FSR photon conversions and in-flight heavy-flavor decays constitute the latter. Though the lepton isolation requirement (mentioned in Sec. III A) and the b-jet veto (mentioned later in Sec. III D) significantly

TABLE II. Summary of optimized BDT hyperparameters.

BDT hyperparameter	Optimized choice
NTrees	1000
MinNodeSize	5%
MaxDepth	4
BoostType	AdaBoost
AdaBoostBeta	0.1
UseBaggedBoost	True
BaggedSampleFraction	0.5
SeparationType	GiniIndex
nCuts	−1

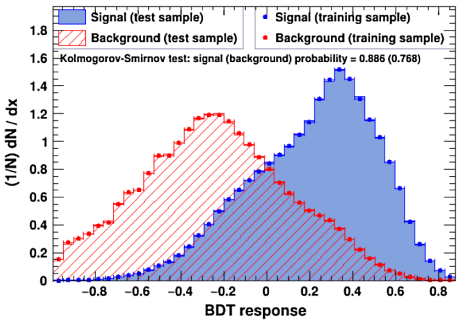

FIG. 6. BDT response curves for the training and testing subsamples.

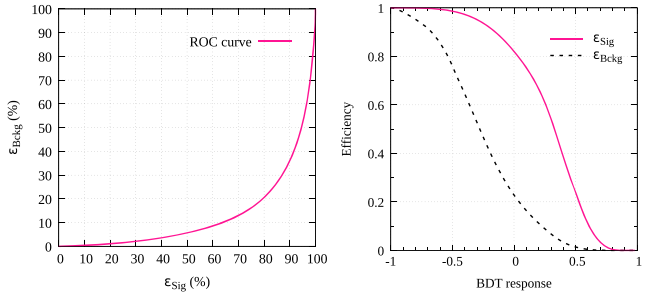

FIG. 7. BDT performance in terms of the ROC curve (left) and the signal (with $m_{H^{\pm\pm}} = 150$ GeV) and background efficiencies as a function of the BDT response.

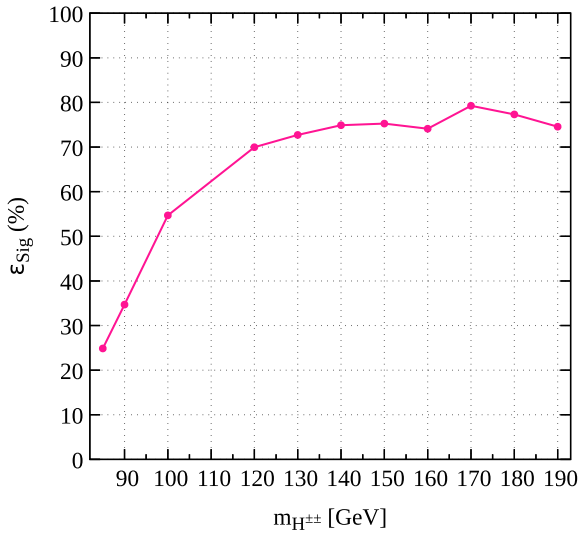

FIG. 8. The signal efficiency as a function of $m_{H^{\pm\pm}}$ for the BDT response of 0.1.

subdue the latter, a considerable fraction of this still passes the object selection. The estimation of this contribution requires a data-driven approach, namely, the so-called *fake factor* method, which is beyond the realm of this work. We adopt a conservative approach, assuming a p_T-dependent probability of 0.1–0.3% for a jet to be misidentified as a lepton [117]. Further, to account for the electron charge misidentification due to their bremsstrahlung interactions with the inner detector material, all prompt electrons are naively corrected with a p_T- and η-dependent charge misidentification probability: $P(p_T, \eta) = \sigma(p_T) \times f(\eta)$, where $\sigma(p_T)$ and $f(\eta)$ range from 0.02 to 0.1 and 0.03 to 1, respectively [118].

D. Event selection and analysis

Here, we discuss the selection criteria that are adept in ameliorating the signal-to-background ratio. Only the events satisfying the following selection cuts (*S0*) are considered for further analysis:

(1) one fat jet with $p_T > 300$ GeV,
(2) two same-sign leptons,
(3) the angular separation between the leptons $\Delta R_{\ell\ell} > 0.05$, and
(4) the dilepton invariant mass $m_{\ell\ell} > 1$ GeV as well as $m_{\ell\ell} \notin [3, 3.2]$ GeV.

The requirements $\Delta R_{\ell\ell} > 0.05$ and $m_{\ell\ell} > 1$ GeV vanquish the background contributions from muon bremsstrahlung interactions as well as ISR/FSR photon conversions, and $m_{\ell\ell} \notin [3, 3.2]$ GeV suppresses contributions from J/ψ decays.

The events satisfying the *S0* cut are then fed to the trained BDT classifier described in Sec. III B. Following the discussion in Sec. III B, we impose a modest cut on the BDT response:

$$S1\text{: BDT response} > 0.1.$$

Figure 9 shows the normalized distribution of $m_{\ell\ell}$ for the signal with $m_{H^{\pm\pm}} = 150$ GeV and background events satisfying the *S1* cut. For the signal, it is a monotonically falling distribution with an end point near 120 GeV as occasioned by the low mass of $H^{\pm\pm}$. On the contrary, the background boasts a peak at the Z-boson mass with the lion's share of the contributions accruing from $Z \to e^- e^+$ when one of the electrons charge get misidentified. To suppress the $Z \to e^- e^+$ contribution, we require that

$$S2\text{: } m_{\ell\ell} < 80 \text{ GeV}.$$

In the second panel of Fig. 9, displayed is the normalized distribution for p_T^{miss}, suggesting that the signal looks much harder than the background. Therefore, a reasonably strong cut on p_T^{miss} would be helpful in curtailing the latter without impinging much on the former. In Fig. 9, also displayed are the distributions for the angular separation between the two leptons ($\Delta R_{\ell\ell}$) and the azimuthal separation between the dilepton system and p_T^{miss} ($\Delta\phi(\ell\ell, p_T^{\text{miss}})$). As we see, unlike the background, most of the signal events are contained within $\Delta R_{\ell\ell} \sim 1$ and $\Delta\phi(\ell\ell, p_T^{\text{miss}}) \sim 1$ showing that, as we expect, the leptons and neutrinos emanating from highly Lorentz-boosted $H^{\pm\pm}$ are adjacent to each

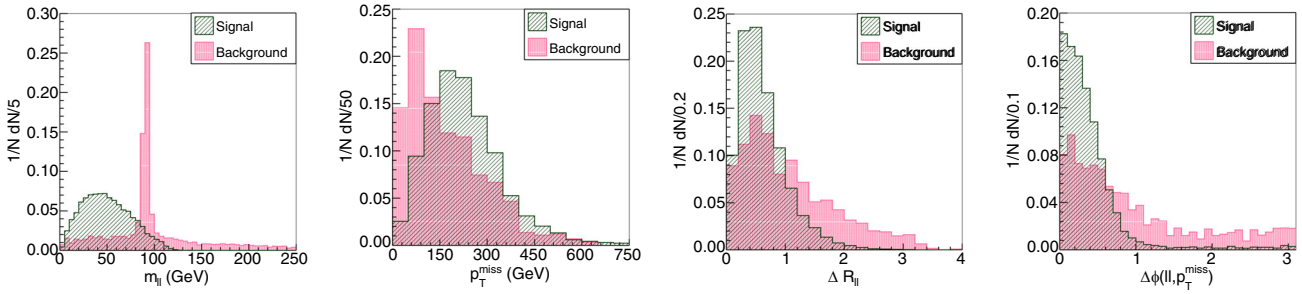

FIG. 9. Normalized distribution for the signal with $m_{H^{\pm\pm}} = 150$ GeV and background events. (From the left to right) first: $m_{\ell\ell}$ after the S1 cut; second, third, and fourth: $p_T^{\rm miss}$, $\Delta R_{\ell\ell}$, and $\Delta\phi(\ell\ell, p_T^{\rm miss})$, respectively, after the S2 cut.

other. Guided by these distributions, we impose the following set of cuts:

$$S3\colon\ \Delta R_{\ell\ell} < 1.2, \quad p_T^{\rm miss} > 80\ {\rm GeV}, \quad \Delta\phi(\ell\ell, p_T^{\rm miss}) < 0.8.$$

Table III shows the progression of the background and signal (with $m_{H^{\pm\pm}} = 90$, 120, and 150 GeV) cross sections at the 13 TeV LHC as subsequent selection cuts are imposed. As we see, all these cuts turn out be very efficacious in subjugating the background while keeping the signal relatively less harmed.

E. Discovery and exclusion projection

Next, we estimate the discovery and exclusion projection for different $m_{H^{\pm\pm}}$. Following Refs. [119–121], we use the approximated expressions for the median expected discovery and exclusion significances,

$$Z_{\rm dis} = \left[2\left((s+b)\ln\left[\frac{(s+b)(b+\delta_b^2)}{b^2+(s+b)\delta_b^2}\right] - \frac{b^2}{\delta_b^2}\ln\left[1+\frac{\delta_b^2 s}{b(b+\delta_b^2)}\right]\right)\right]^{1/2}, \tag{7}$$

TABLE III. Signal and background cross sections (fb) after different selection cuts.

Event sample	*S0*	*S1*	*S2*	*S3*
γ^*/Z^*	11.49	2.432	0.154	0.004
$t\bar{t}$	3.931	0.436	0.120	0.028
$W^\pm Z$	3.238	0.784	0.216	0.057
$t\bar{t}W^\pm$	2.461	0.311	0.084	0.018
$W^\pm W^\pm jj$	1.992	0.480	0.107	0.023
$W^\pm$	1.985	0.473	0.334	0.116
$W^\pm W^\pm W^\mp$	1.474	0.284	0.076	0.022
Others	3.579	0.598	0.168	0.046
Total background	30.15	5.798	1.259	0.314
Signal: $m_{H^{\pm\pm}} = 90$ GeV	0.946	0.387	0.387	0.312
Signal: $m_{H^{\pm\pm}} = 120$ GeV	1.087	0.735	0.731	0.586
Signal: $m_{H^{\pm\pm}} = 150$ GeV	0.976	0.652	0.560	0.434

$$Z_{\rm exc} = \left[2\left\{s - b\ln\left(\frac{b+s+x}{2b}\right) - \frac{b^2}{\delta_b^2}\ln\left(\frac{b-s+x}{2b}\right)\right\} - (b+s-x)(1+b/\delta_b^2)\right]^{1/2}, \tag{8}$$

where $x = \sqrt{(s+b)^2 - 4sb\delta_b^2/(b+\delta_b^2)}$; s and b are the number of signal and background events, respectively; and δ_b is the uncertainty in the measurement of the background.

The estimation of the background uncertainty arising from several sources such as the reconstruction, identification, isolation, and trigger efficiency; the energy scale and resolution of different physics objects; the luminosity measurements; the pileup modeling; the parton-shower modeling; the higher-order QCD corrections; etc. is beyond the scope of this work. We adopt a conservative approach, following the typical LHC searches [122,123], for which both the theoretical and experimental uncertainties are $\mathcal{O}(10)\%$ each, and we assume an overall 20% total uncertainty for the same.

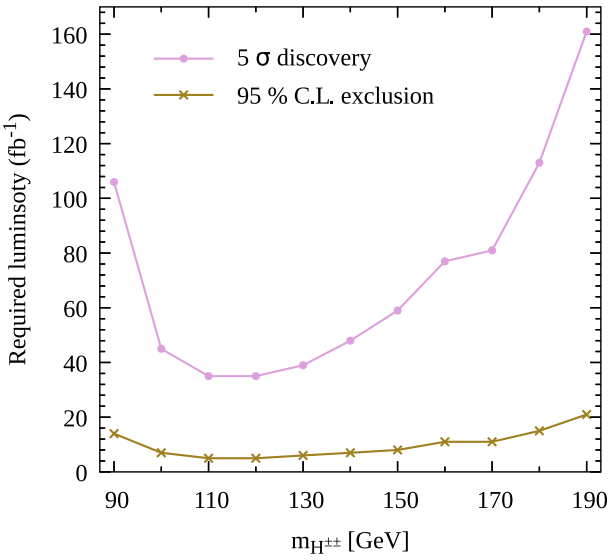

FIG. 10. Required luminosity (fb^{-1}) for the 5σ discovery and 95% exclusion for different $m_{H^{\pm\pm}}$.

In Fig. 10, we show the required luminosities (in fb^{-1}) needed to achieve a median expected $Z_{\text{exc}} \geq 1.645$ (95% C.L. exclusion) as well as $Z_{\text{dis}} \geq 5$ (5σ discovery) for different $m_{H^{\pm\pm}}$. The rise in the required luminosity for $m_{H^{\pm\pm}} \lesssim 100$ GeV could be attributed to, as discussed in the end of Sec. III B, the poor separation between the $H^{\pm\pm}$ jets and the SM jets, whereas that for larger masses is due to the fall in the signal cross section (see Fig. 2).

We find that $H^{\pm\pm}$ within the [84,200] GeV mass range could be probed with 5σ discovery significance with the already collected Run 2 LHC data. On the other hand, in the case of the data found to be consistent with the SM background, only a fraction of the collected data suffices to exclude them at 95% C.L.

IV. SUMMARY

Doubly charged Higgs bosons within the mass range 84–200 GeV decaying into a pair of W bosons have been overlooked by the LHC searches. Lately, Refs. [75–78] have demonstrated that the recently reported measurement of the W-bosoon mass by the CDF experiment can be accommodated within the type-II seesaw model predicting such low-mass $H^{\pm\pm}$ and slightly heavier singly-charged and neutral scalars. In view of this, it has been paramount to look for such $H^{\pm\pm}$ at the LHC. In this work, we have presented a novel search strategy for such $H^{\pm\pm}$ considering their pair production in a highly Lorentz-boosted regime such that they are produced back to back with large transverse momenta, manifesting as a single fat jet or a pair of adjacent same-sign leptons plus missing transverse momentum. First, we perform a multivariate analysis to discern such exotic $H^{\pm\pm}$ jets from the SM jets. Then, we perform a search in the final state with an $H^{\pm\pm}$ jet and two same-sign leptons plus missing transverse momentum. We find that such low-mass $H^{\pm\pm}$ could be directly probed with the already collected Run 2 LHC data.

In closing this section, we mention that the search strategy presented here is applicable to any low-mass beyond the SM Higgses (charged as well as neutral) decaying into a pair of SM gauge bosons.

ACKNOWLEDGMENTS

S. A. and K. G. acknowledge the SERB Core Research Grants No. CRG/2018/004889 and No. CRG/2019/006831, respectively. The simulations were supported in part by the SAMKHYA: High Performance Computing Facility provided by Institute of Physics, Bhubaneswar.

Note added.—Recently, an article [124] with similar motivation appeared on the arXiv, concluding that most of the favored space for the CDF discrepancy is already excluded by the existing LHC Run 2 data. While our proposed search strategy is completely different from Ref. [124], we also arrived at a similar conclusion that the already collected LHC Run 2 data are sufficient to probe low-mass doubly charged Higgs bosons in the type-II seesaw model. Moreover, our strategy is applicable to any low-mass beyond the SM Higgses (charged as well as neutral) decaying into a pair of SM gauge bosons.

[1] W. Konetschny and W. Kummer, Nonconservation of total lepton number with scalar bosons, Phys. Lett. **70B**, 433 (1977).
[2] T. P. Cheng and L.-F. Li, Neutrino masses, mixings and oscillations in SU(2) × U(1) models of electroweak interactions, Phys. Rev. D **22**, 2860 (1980).
[3] G. Lazarides, Q. Shafi, and C. Wetterich, Proton lifetime and fermion masses in an SO(10) model, Nucl. Phys. **B181**, 287 (1981).
[4] J. Schechter and J. W. F. Valle, Neutrino masses in SU(2) × U(1) theories, Phys. Rev. D **22**, 2227 (1980).
[5] R. N. Mohapatra and G. Senjanovic, Neutrino masses and mixings in gauge models with spontaneous parity violation, Phys. Rev. D **23**, 165 (1981).
[6] M. Magg and C. Wetterich, Neutrino mass problem and gauge hierarchy, Phys. Lett. **94B**, 61 (1980).
[7] S. Weinberg, Baryon and Lepton Nonconserving Processes, Phys. Rev. Lett. **43**, 1566 (1979).
[8] E. Ma, Pathways to Naturally Small Neutrino Masses, Phys. Rev. Lett. **81**, 1171 (1998).
[9] K. Huitu, J. Maalampi, A. Pietila, and M. Raidal, Doubly charged Higgs at LHC, Nucl. Phys. **B487**, 27 (1997).
[10] J. F. Gunion, C. Loomis, and K. T. Pitts, Searching for doubly charged Higgs bosons at future colliders, eConf **C960625**, LTH096 (1996), arXiv:hep-ph/9610237.
[11] S. Chakrabarti, D. Choudhury, R. M. Godbole, and B. Mukhopadhyaya, Observing doubly charged Higgs bosons in photon-photon collisions, Phys. Lett. B **434**, 347 (1998).
[12] E. J. Chun, K. Y. Lee, and S. C. Park, Testing Higgs triplet model and neutrino mass patterns, Phys. Lett. B **566**, 142 (2003).
[13] M. Muhlleitner and M. Spira, A note on doubly charged Higgs pair production at hadron colliders, Phys. Rev. D **68**, 117701 (2003).
[14] A. G. Akeroyd and M. Aoki, Single and pair production of doubly charged Higgs bosons at hadron colliders, Phys. Rev. D **72**, 035011 (2005).
[15] A. G. Akeroyd, M. Aoki, and H. Sugiyama, Probing Majorana phases and neutrino mass spectrum in the Higgs

triplet model at the CERN LHC, Phys. Rev. D **77**, 075010 (2008).
[16] J. Garayoa and T. Schwetz, Neutrino mass hierarchy and Majorana *CP* phases within the Higgs triplet model at the LHC, J. High Energy Phys. 03 (2008) 009.
[17] T. Han, B. Mukhopadhyaya, Z. Si, and K. Wang, Pair production of doubly charged scalars: Neutrino mass constraints and signals at the LHC, Phys. Rev. D **76**, 075013 (2007).
[18] M. Kadastik, M. Raidal, and L. Rebane, Direct determination of neutrino mass parameters at future colliders, Phys. Rev. D **77**, 115023 (2008).
[19] F. del Aguila and J. A. Aguilar-Saavedra, Distinguishing seesaw models at LHC with multi-lepton signals, Nucl. Phys. **B813**, 22 (2009).
[20] P. Fileviez Perez, T. Han, G.-y. Huang, T. Li, and K. Wang, Neutrino masses and the CERN LHC: Testing type II seesaw, Phys. Rev. D **78**, 015018 (2008).
[21] A. G. Akeroyd and C.-W. Chiang, Doubly charged Higgs bosons and three-lepton signatures in the Higgs Triplet Model, Phys. Rev. D **80**, 113010 (2009).
[22] A. G. Akeroyd, C.-W. Chiang, and N. Gaur, Leptonic signatures of doubly charged Higgs boson production at the LHC, J. High Energy Phys. 11 (2010) 005.
[23] A. Arhrib, R. Benbrik, M. Chabab, G. Moultaka, M. C. Peyranere, L. Rahili, and J. Ramadan, The Higgs potential in the type II seesaw model, Phys. Rev. D **84**, 095005 (2011).
[24] A. Melfo, M. Nemevsek, F. Nesti, G. Senjanovic, and Y. Zhang, Type II seesaw at LHC: The roadmap, Phys. Rev. D **85**, 055018 (2012).
[25] M. Aoki, S. Kanemura, and K. Yagyu, Testing the Higgs triplet model with the mass difference at the LHC, Phys. Rev. D **85**, 055007 (2012).
[26] A. G. Akeroyd and H. Sugiyama, Production of doubly charged scalars from the decay of singly charged scalars in the Higgs Triplet Model, Phys. Rev. D **84**, 035010 (2011).
[27] F. Arbabifar, S. Bahrami, and M. Frank, Neutral Higgs bosons in the Higgs Triplet Model with nontrivial mixing, Phys. Rev. D **87**, 015020 (2013).
[28] C.-W. Chiang, T. Nomura, and K. Tsumura, Search for doubly charged Higgs bosons using the same-sign diboson mode at the LHC, Phys. Rev. D **85**, 095023 (2012).
[29] A. G. Akeroyd, S. Moretti, and H. Sugiyama, Five-lepton and six-lepton signatures from production of neutral triplet scalars in the Higgs Triplet Model, Phys. Rev. D **85**, 055026 (2012).
[30] E. J. Chun, H. M. Lee, and P. Sharma, Vacuum stability, perturbativity, EWPD and Higgs-to-diphoton rate in type II seesaw models, J. High Energy Phys. 11 (2012) 106.
[31] E. J. Chun and P. Sharma, Same-sign tetra-leptons from type II seesaw, J. High Energy Phys. 08 (2012) 162.
[32] F. del Águila and M. Chala, LHC bounds on lepton number violation mediated by doubly and singly-charged scalars, J. High Energy Phys. 03 (2014) 027.
[33] E. J. Chun and P. Sharma, Search for a doubly charged boson in four lepton final states in type II seesaw, Phys. Lett. B **728**, 256 (2014).
[34] S. Kanemura, K. Yagyu, and H. Yokoya, First constraint on the mass of doubly charged Higgs bosons in the same-sign diboson decay scenario at the LHC, Phys. Lett. B **726**, 316 (2013).
[35] P. S. Bhupal Dev, D. K. Ghosh, N. Okada, and I. Saha, 125 GeV Higgs boson and the type-II seesaw model, J. High Energy Phys. 03 (2013) 150; Erratum, J. High Energy Phys. 05 (2013) 049.
[36] S. Kanemura, M. Kikuchi, K. Yagyu, and H. Yokoya, Bounds on the mass of doubly charged Higgs bosons in the same-sign diboson decay scenario, Phys. Rev. D **90**, 115018 (2014).
[37] S. Kanemura, M. Kikuchi, H. Yokoya, and K. Yagyu, LHC Run-I constraint on the mass of doubly charged Higgs bosons in the same-sign diboson decay scenario, Prog. Theor. Exp. Phys. **2015**, 051B02 (2015).
[38] Z. Kang, J. Li, T. Li, Y. Liu, and G.-Z. Ning, Light doubly charged Higgs boson via the WW^* channel at LHC, Eur. Phys. J. C **75**, 574 (2015).
[39] F. F. Deppisch, P. S. Bhupal Dev, and A. Pilaftsis, Neutrinos and collider physics, New J. Phys. **17**, 075019 (2015).
[40] Z.-L. Han, R. Ding, and Y. Liao, LHC phenomenology of type II seesaw: Nondegenerate case, Phys. Rev. D **91**, 093006 (2015).
[41] Z.-L. Han, R. Ding, and Y. Liao, LHC phenomenology of the type II seesaw mechanism: Observability of neutral scalars in the nondegenerate case, Phys. Rev. D **92**, 033014 (2015).
[42] S. Blunier, G. Cottin, M. A. Díaz, and B. Koch, Phenomenology of a Higgs triplet model at future e^+e^- colliders, Phys. Rev. D **95**, 075038 (2017).
[43] D. Das and A. Santamaria, Updated scalar sector constraints in the Higgs triplet model, Phys. Rev. D **94**, 015015 (2016).
[44] M. Mitra, S. Niyogi, and M. Spannowsky, Type-II seesaw model and multilepton signatures at hadron colliders, Phys. Rev. D **95**, 035042 (2017).
[45] Y. Cai, T. Han, T. Li, and R. Ruiz, Lepton number violation: Seesaw models and their collider tests, Front. Phys. **6**, 40 (2018).
[46] D. K. Ghosh, N. Ghosh, I. Saha, and A. Shaw, Revisiting the high-scale validity of the type II seesaw model with novel LHC signature, Phys. Rev. D **97**, 115022 (2018).
[47] T. Nomura, H. Okada, and H. Yokoya, Discriminating leptonic Yukawa interactions with doubly charged scalar at the ILC, Nucl. Phys. **B929**, 193 (2018).
[48] S. Antusch, O. Fischer, A. Hammad, and C. Scherb, Low scale type II seesaw: Present constraints and prospects for displaced vertex searches, J. High Energy Phys. 02 (2019) 157.
[49] P. S. Bhupal Dev and Y. Zhang, Displaced vertex signatures of doubly charged scalars in the type-II seesaw and its left-right extensions, J. High Energy Phys. 10 (2018) 199.
[50] A. Crivellin, M. Ghezzi, L. Panizzi, G. M. Pruna, and A. Signer, Low- and high-energy phenomenology of a doubly charged scalar, Phys. Rev. D **99**, 035004 (2019).
[51] P. Agrawal, M. Mitra, S. Niyogi, S. Shil, and M. Spannowsky, Probing the type-II seesaw mechanism through the production of Higgs bosons at a lepton collider, Phys. Rev. D **98**, 015024 (2018).

[52] L. Rahili, A. Arhrib, and R. Benbrik, Associated production of SM Higgs with a photon in type-II seesaw models at the ILC, Eur. Phys. J. C **79**, 940 (2019).
[53] T. B. de Melo, F. S. Queiroz, and Y. Villamizar, Doubly charged scalar at the high-luminosity and high-energy LHC, Int. J. Mod. Phys. A **34**, 1950157 (2019).
[54] P. S. B. Dev, S. Khan, M. Mitra, and S. K. Rai, Doubly charged Higgs boson at a future electron-proton collider, Phys. Rev. D **99**, 115015 (2019).
[55] R. Primulando, J. Julio, and P. Uttayarat, Scalar phenomenology in type-II seesaw model, J. High Energy Phys. 08 (2019) 024.
[56] E. J. Chun, S. Khan, S. Mandal, M. Mitra, and S. Shil, Same-sign tetralepton signature at the Large Hadron Collider and a future pp collider, Phys. Rev. D **101**, 075008 (2020).
[57] R. Padhan, D. Das, M. Mitra, and A. Kumar Nayak, Probing doubly and singly charged Higgs bosons at the pp collider HE-LHC, Phys. Rev. D **101**, 075050 (2020).
[58] P. Bandyopadhyay, A. Karan, and C. Sen, Discerning signatures of seesaw models and complementarity of leptonic colliders, arXiv:2011.04191.
[59] J. Gluza, M. Kordiaczynska, and T. Srivastava, Discriminating the HTM and MLRSM models in collider studies via doubly charged Higgs boson pair production and the subsequent leptonic decays, Chin. Phys. C **45**, 073113 (2021).
[60] S. Ashanujjaman and K. Ghosh, Revisiting type-II seesaw: Present limits and future prospects at LHC, J. High Energy Phys. 03 (2022) 195.
[61] X.-H. Yang and Z.-J. Yang, Doubly charged Higgs production at future ep colliders, Chin. Phys. C **46**, 063107 (2022).
[62] S. Ashanujjaman, K. Ghosh, and K. Huitu, Type-II see-saw: Searching the LHC elusive low-mass triplet-like Higgses at e^-e^+ colliders, Phys. Rev. D **106**, 075028 (2022).
[63] G. Aad *et al.* (ATLAS Collaboration), Search for doubly charged Higgs bosons in like-sign dilepton final states at $\sqrt{s} = 7$ TeV with the ATLAS detector, Eur. Phys. J. C **72**, 2244 (2012).
[64] S. Chatrchyan *et al.* (CMS Collaboration), A search for a doubly charged Higgs boson in pp collisions at $\sqrt{s} = 7$ TeV, Eur. Phys. J. C **72**, 2189 (2012).
[65] G. Aad *et al.* (ATLAS Collaboration), Search for anomalous production of prompt same-sign lepton pairs and pair-produced doubly charged Higgs bosons with $\sqrt{s} = 8$ TeV pp collisions using the ATLAS detector, J. High Energy Phys. 03 (2015) 041.
[66] V. Khachatryan *et al.* (CMS Collaboration), Study of Vector Boson Scattering and Search for New Physics in Events with Two Same-Sign Leptons and Two Jets, Phys. Rev. Lett. **114**, 051801 (2015).
[67] CMS Collaboration, Search for a doubly charged Higgs boson with $\sqrt{s} = 8$ TeV pp collisions at the CMS experiment, Report No. CMS-PAS-HIG-14-039 (2016), http://cds.cern.ch/record/2127498.
[68] CMS Collaboration, A search for doubly charged Higgs boson production in three and four lepton final states at $\sqrt{s} = 13$ TeV, Report No. CMS-PAS-HIG-16-036 (2017), https://cds.cern.ch/record/2242956.
[69] M. Aaboud *et al.* (ATLAS Collaboration), Search for doubly charged Higgs boson production in multi-lepton final states with the ATLAS detector using proton–proton collisions at $\sqrt{s} = 13$ TeV, Eur. Phys. J. C **78**, 199 (2018).
[70] A. M. Sirunyan *et al.* (CMS Collaboration), Observation of Electroweak Production of Same-Sign W Boson Pairs in the Two Jet and Two Same-Sign Lepton Final State in Proton-Proton Collisions at $\sqrt{s} = 13$ TeV, Phys. Rev. Lett. **120**, 081801 (2018).
[71] M. Aaboud *et al.* (ATLAS Collaboration), Search for doubly charged scalar bosons decaying into same-sign W boson pairs with the ATLAS detector, Eur. Phys. J. C **79**, 58 (2019).
[72] G. Aad *et al.* (ATLAS Collaboration), Search for doubly and singly charged Higgs bosons decaying into vector bosons in multi-lepton final states with the ATLAS detector using proton-proton collisions at $\sqrt{s} = 13$ TeV, J. High Energy Phys. 06 (2021) 146.
[73] ATLAS Collaboration, Search for doubly charged Higgs boson production in multi-lepton final states using 139 fb^{-1} of proton–proton collisions at $\sqrt{s} = 13$ TeV with the ATLAS detector, Report No. CERN-EP-2022-212 (2022).
[74] Z. Kang, J. Li, T. Li, Y. Liu, and G.-Z. Ning, Light doubly charged Higgs boson via the WW^* channel at LHC, Eur. Phys. J. C **75**, 574 (2015).
[75] S. Kanemura and K. Yagyu, Implication of the W boson mass anomaly at CDF II in the Higgs triplet model with a mass difference, Phys. Lett. B **831**, 137217 (2022).
[76] J. Heeck, W-boson mass in the triplet seesaw model, Phys. Rev. D **106**, 015004 (2022).
[77] H. Bahl, W. H. Chiu, C. Gao, L.-T. Wang, and Y.-M. Zhong, Tripling down on the W boson mass, Eur. Phys. J. C **82**, 944 (2022).
[78] Y. Cheng, X.-G. He, F. Huang, J. Sun, and Z.-P. Xing, Electroweak precision tests for triplet scalars, arXiv:2208.06760.
[79] T. Aaltonen *et al.* (CDF Collaboration), High-precision measurement of the W boson mass with the CDF II detector, Science **376**, 170 (2022).
[80] M. Awramik, M. Czakon, A. Freitas, and G. Weiglein, Precise prediction for the W boson mass in the standard model, Phys. Rev. D **69**, 053006 (2004).
[81] T.-K. Chen, C.-W. Chiang, and K. Yagyu, Explanation of the W mass shift at CDF II in the extended Georgi-Machacek model, Phys. Rev. D **106**, 055035 (2022).
[82] R. Ghosh, B. Mukhopadhyaya, and U. Sarkar, The ρ parameter and the CDF W-mass anomaly: observations on the role of scalar triplets, arXiv:2205.05041.
[83] F. Staub, SARAH 4: A tool for (not only SUSY) model builders, Comput. Phys. Commun. **185**, 1773 (2014).
[84] F. Staub, Exploring new models in all detail with SARAH, Adv. High Energy Phys. **2015**, 840780 (2015).
[85] C. Degrande, C. Duhr, B. Fuks, D. Grellscheid, O. Mattelaer, and T. Reiter, UFO—The universal FeynRules output, Comput. Phys. Commun. **183**, 1201 (2012).
[86] J. Alwall, M. Herquet, F. Maltoni, O. Mattelaer, and T. Stelzer, MadGraph 5: Going beyond, J. High Energy Phys. 06 (2011) 128.

[87] J. Alwall, R. Frederix, S. Frixione, V. Hirschi, F. Maltoni, O. Mattelaer, H. S. Shao, T. Stelzer, P. Torrielli, and M. Zaro, The automated computation of tree-level and next-to-leading order differential cross sections, and their matching to parton shower simulations, J. High Energy Phys. 07 (2014) 079.
[88] R. D. Ball, V. Bertone, S. Carrazza, L. Del Debbio, S. Forte, A. Guffanti, N. P. Hartland, and J. Rojo (NNPDF Collaboration), Parton distributions with QED corrections, Nucl. Phys. **B877**, 290 (2013).
[89] R. D. Ball *et al.* (NNPDF Collaboration), Parton distributions for the LHC Run II, J. High Energy Phys. 04 (2015) 040.
[90] B. Fuks, M. Nemevšek, and R. Ruiz, Doubly charged Higgs boson production at hadron colliders, Phys. Rev. D **101**, 075022 (2020).
[91] T. Sjöstrand, S. Ask, J. R. Christiansen, R. Corke, N. Desai, P. Ilten, S. Mrenna, S. Prestel, C. O. Rasmussen, and P. Z. Skands, An introduction to PYTHIA 8.2, Comput. Phys. Commun. **191**, 159 (2015).
[92] J. de Favereau, C. Delaere, P. Demin, A. Giammanco, V. Lemaître, A. Mertens, and M. Selvaggi (DELPHES 3 Collaboration), DELPHES 3, A modular framework for fast simulation of a generic collider experiment, J. High Energy Phys. 02 (2014) 057.
[93] M. Cacciari, G. P. Salam, and G. Soyez, The anti-k_t jet clustering algorithm, J. High Energy Phys. 04 (2008) 063.
[94] M. Cacciari, G. P. Salam, and G. Soyez, FastJet user manual, Eur. Phys. J. C **72**, 1896 (2012).
[95] S. D. Ellis, C. K. Vermilion, and J. R. Walsh, Techniques for improved heavy particle searches with jet substructure, Phys. Rev. D **80**, 051501 (2009).
[96] S. D. Ellis, C. K. Vermilion, and J. R. Walsh, Recombination algorithms and jet substructure: Pruning as a tool for heavy particle searches, Phys. Rev. D **81**, 094023 (2010).
[97] J. Thaler and K. Van Tilburg, Identifying boosted objects with N-subjettiness, J. High Energy Phys. 03 (2011) 015.
[98] J. Thaler and K. Van Tilburg, Maximizing boosted top identification by minimizing N-subjettiness, J. High Energy Phys. 02 (2012) 093.
[99] A. Hocker *et al.*, TMVA—Toolkit for multivariate data analysis, arXiv:physics/0703039.
[100] R. Brun, F. Rademakers, ROOT, an object oriented data analysis framework, Nucl. Instrum. Methods Phys. Res., Sect. A **389**, 81 (2000).
[101] D. Krohn, M. D. Schwartz, T. Lin, and W. J. Waalewijn, Jet Charge at the LHC, Phys. Rev. Lett. **110**, 212001 (2013).
[102] S. Catani, L. Cieri, G. Ferrera, D. de Florian, and M. Grazzini, Vector Boson Production at Hadron Colliders: A Fully Exclusive QCD Calculation at NNLO, Phys. Rev. Lett. **103**, 082001 (2009).
[103] G. Balossini, G. Montagna, C. M. Carloni Calame, M. Moretti, O. Nicrosini, F. Piccinini, M. Treccani, and A. Vicini, Combination of electroweak and QCD corrections to single W production at the Fermilab Tevatron and the CERN LHC, J. High Energy Phys. 01 (2010) 013.
[104] J. M. Campbell, R. K. Ellis, and C. Williams, Vector boson pair production at the LHC, J. High Energy Phys. 07 (2011) 018.
[105] F. Cascioli, T. Gehrmann, M. Grazzini, S. Kallweit, P. Maierhöfer, A. von Manteuffel, S. Pozzorini, D. Rathlev, L. Tancredi, and E. Weihs, ZZ production at hadron colliders in NNLO QCD, Phys. Lett. B **735**, 311 (2014).
[106] J. M. Campbell, R. K. Ellis, and C. Williams, Associated production of a Higgs boson at NNLO, J. High Energy Phys. 06 (2016) 179.
[107] D. de Florian *et al.* (LHC Higgs Cross Section Working Group), Handbook of LHC Higgs cross sections: 4. Deciphering the nature of the Higgs sector, arXiv:1610.07922.
[108] Y.-B. Shen, R.-Y. Zhang, W.-G. Ma, X.-Z. Li, and L. Guo, NLO QCD and electroweak corrections to WWW production at the LHC, Phys. Rev. D **95**, 073005 (2017).
[109] D. T. Nhung, L. D. Ninh, and M. M. Weber, NLO corrections to WWZ production at the LHC, J. High Energy Phys. 12 (2013) 096.
[110] Y.-B. Shen, R.-Y. Zhang, W.-G. Ma, X.-Z. Li, Y. Zhang, and L. Guo, NLO QCD + NLO EW corrections to *WZZ* productions with leptonic decays at the LHC, J. High Energy Phys. 10 (2015) 186; Erratum, J. High Energy Phys. 10 (2016) 156.
[111] H. Wang, R.-Y. Zhang, W.-G. Ma, L. Guo, X.-Z. Li, and S.-M. Wang, NLO QCD + EW corrections to ZZZ production with subsequent leptonic decays at the LHC, J. Phys. G **43**, 115001 (2016).
[112] R. Frederix, S. Frixione, V. Hirschi, F. Maltoni, O. Mattelaer, P. Torrielli, E. Vryonidou, and M. Zaro, Higgs pair production at the LHC with NLO and parton-shower effects, Phys. Lett. B **732**, 142 (2014).
[113] N. Kidonakis, Theoretical results for electroweak-boson and single-top production, Proc. Sci. DIS2015 (**2015**) 170.
[114] C. Muselli, M. Bonvini, S. Forte, S. Marzani, and G. Ridolfi, Top quark pair production beyond NNLO, J. High Energy Phys. 08 (2015) 076.
[115] A. Broggio, A. Ferroglia, R. Frederix, D. Pagani, B. D. Pecjak, and I. Tsinikos, Top-quark pair hadroproduction in association with a heavy boson at NLO + NNLL including EW corrections, J. High Energy Phys. 08 (2019) 039.
[116] R. Frederix, D. Pagani, and M. Zaro, Large NLO corrections in $t\bar{t}W^{\pm}$ and $t\bar{t}t\bar{t}$ hadroproduction from supposedly subleading EW contributions, J. High Energy Phys. 02 (2018) 031.
[117] ATLAS Collaboration, Electron efficiency measurements with the ATLAS detector using the 2015 LHC proton-proton collision data, Report No. ATLAS-CONF-2016-024 (2016), http://cds.cern.ch/record/2157687.
[118] M. Aaboud *et al.* (ATLAS Collaboration), Search for doubly charged Higgs boson production in multi-lepton final states with the ATLAS detector using proton–proton collisions at $\sqrt{s} = 13$ TeV, Eur. Phys. J. C **78**, 199 (2018).
[119] G. Cowan, K. Cranmer, E. Gross, and O. Vitells, Asymptotic formulae for likelihood-based tests of new physics, Eur. Phys. J. C **71**, 1554 (2011); Erratum, Eur. Phys. J. C **73**, 2501 (2013).
[120] T. P. Li and Y. Q. Ma, Analysis methods for results in gamma-ray astronomy, Astrophys. J. **272**, 317 (1983).
[121] R. D. Cousins, J. T. Linnemann, and J. Tucker, Evaluation of three methods for calculating statistical significance when incorporating a systematic uncertainty into a test of

the background-only hypothesis for a Poisson process, Nucl. Instrum. Methods Phys. Res., Sect. A **595**, 480 (2008).

[122] A. M. Sirunyan *et al.* (CMS Collaboration), Search for physics beyond the standard model in multilepton final states in proton-proton collisions at $\sqrt{s} = 13$ TeV, J. High Energy Phys. 03 (2020) 051.

[123] ATLAS Collaboration, Search for new phenomena in three- or four-lepton events in pp collisions at $\sqrt{s} = 13$ TeV with the ATLAS detector, Report No. ATLAS-CONF-2021-011 (2021).

[124] J. Butterworth, J. Heeck, S. H. Jeon, O. Mattelaer, and R. Ruiz, Testing the scalar triplet solution to CDF's fat W problem at the LHC, arXiv:2210.13496.